



SETCOR
Conferences & Exhibitions

**The 6th edition of Nanotech France 2021
International Conference**

Nanotech France 2021

**Held Virtually - June 23 to 25, 2021
Conference Proceedings**

DOI: <https://doi.org/10.26799/cp-nanotechfrance2021>

Comb-referenced interferometry in nanopositioning and nanomeasuring machines

Ulrike Blumröder¹, Paul Köchert², Thomas Fröhlich¹, Roland Füßl¹, Ingo Ortlepp¹, Uwe Gerhardt¹, Rostyslav Mastylo¹, Jens Flügge², Harald Bosse² and Eberhard Manske¹

¹Institute of Process Measurement and Sensor Technology, TU Ilmenau, Ehrenbergstraße 29, Ilmenau, Germany, ulrike.blumroeder@tu-ilmenau.de

²Precision Engineering Division, Physikalisch-Technische Bundesanstalt Bundesallee 100, Braunschweig, Germany, paul.koechert@ptb.de

Abstract

This work presents the approach of directly stabilizing the metrology lasers of a long-range nanopositioning and measuring machine to an optical frequency comb. The frequency comb is referenced to a GPS disciplined oscillator. This way a direct and permanent link of the laser frequency to an atomic clock is created allowing direct traceability to the SI meter definition. Furthermore the longterm stability of the individual comb lines can be transferred onto the metrology lasers enhancing their longterm stability by three orders of magnitude.

Keywords: nanopositioning machines, optical frequency comb, He-Ne-laser, traceability

1. Introduction

The increasing impact of nanofabrication techniques in research and industry requires high performance distance measurement and positioning systems to provide resolving capabilities down to the sub-nm-range over several hundred millimetres of measurement range. This can be accomplished by using nanopositioning- and measuring machines (NPMM). The NPMMs can be equipped with a variety of different sensor systems or tip- and laser-based nanofabrication tools making them suitable for a characterization of surface topographies or the realization of new approaches in the design of three-dimensional nanostructures [1,2].

In recent years the next generation of nanopositioning and measuring machines (NPMM) was developed at the TU Ilmenau. The NPMM-200 currently provides a measuring range of 200 mm x 200 mm x 25 mm with a positioning repeatability ≤ 4 nm over the whole measurement area and a positioning resolution of 20 pm [1,3]. This performance sets new demands on the frequency stability of the He-Ne lasers and their corresponding wavelength used as a measuring standard in the underlying fiber-coupled laser interferometers.

Currently the 24 h-longterm frequency stability of these lasers is limited to $2 \cdot 10^{-9}$ resulting in a measurement error of 0.4 nm for a maximum measurement range of 200 mm. Furthermore the absolute frequency of these lasers can change during their lifetime operation due to degradation effects that can cause a drift of the center frequency up to ± 5 MHz / year ($\Delta f/f = 10^{-8}/\text{year}$) [4]. Therefore the metrology lasers of the NPMM-200 have to be periodically measured against a BIPM compliant frequency standard, e.g. an iodine stabilized He-Ne-laser [5], to control their absolute frequency and thus avoid systematic length measurement errors over long-time operation of the NPMM.

To eliminate the influence of frequency fluctuations on interferometric length measurements in the long-range NPMMs, measurement errors due to frequency fluctuations will prospectively have to fall below the electronic resolution limit of the interferometers that can reach up to 5 pm resulting in a relative value of $25 \cdot 10^{-12}$ when the operational range of 200 mm is considered [6]. To additionally control the absolute frequency of the metrology lasers a permanent link to a frequency standard is desirable.

These requirements can be met by means of an optical frequency comb. In this study we present the approach of directly stabilizing a He-Ne laser to an optical frequency comb to create a metrology laser with high power output and an ultrastable, traceable vacuum wavelength for the interferometric length measurements in the NPMM-200.

2. Comb-referenced metrology laser

The basic implementation of a comb-referenced metrology laser is depicted in fig. 1. As an optical frequency comb (OFC) a commercial system (Model:FC1500-250-WG, Menlo Systems) with an additional unit for frequency conversion down to 633 nm is used. The comb is referenced to a GPS disciplined oscillator (GPSDO). The GPSDO uses the signals received from GPS satellites to control the frequency output of a local oscillator. This way the longterm accuracy is given by the GPS signal which is traceable to the UTC (NIST). In our case the manufacturer guarantees a relative accuracy of $8 \cdot 10^{-12}$ in 1s with a relative stability of $4 \cdot 10^{-12}$ in 1s [7].

The current metrology lasers of the NPMM-200 are embodied by a fiber-coupled He-Ne heterodyne source [8]. This heterodyne source consists of two independent commercially available He-Ne lasers (model: SL02/1, SIOS Meßtechnik GmbH) with an output power of approximately 1 mW prior to fiber coupling. One of the lasers of the heterodyne source is used to generate a beat-note with one of the comb modes and serves as a “Secondary Standard”. Due to the low power of a single comb mode (usually below 100 nW) nearly all of the laser power of the secondary standard after fiber coupling is used to generate the beat signal which is measured with an Avalanche photodiode (APD). The beat signal has a limited SNR of 30-35 dB and is processed with a FPGA-based control system based on a phase measurement whereas the resonator length of the He-Ne-laser tube serves as an actuator of the control loop [6]. The second laser of the heterodyne source serves as the actual metrology laser and is locked onto the secondary standard. For this purpose some μW optical power of the secondary standard and the metrology laser are used to create a high SNR beat signal of at least 50 dB that is processed with a FPGA-based control system based on a frequency measurement. The beat frequency can be adjusted between 0.1 – 20 MHz. A detailed description of the control electronics and the locking procedure can be found in [6,8].

The residual power of the metrology laser is then used to feed the two long-range interferometer axes of the NPMM-200.

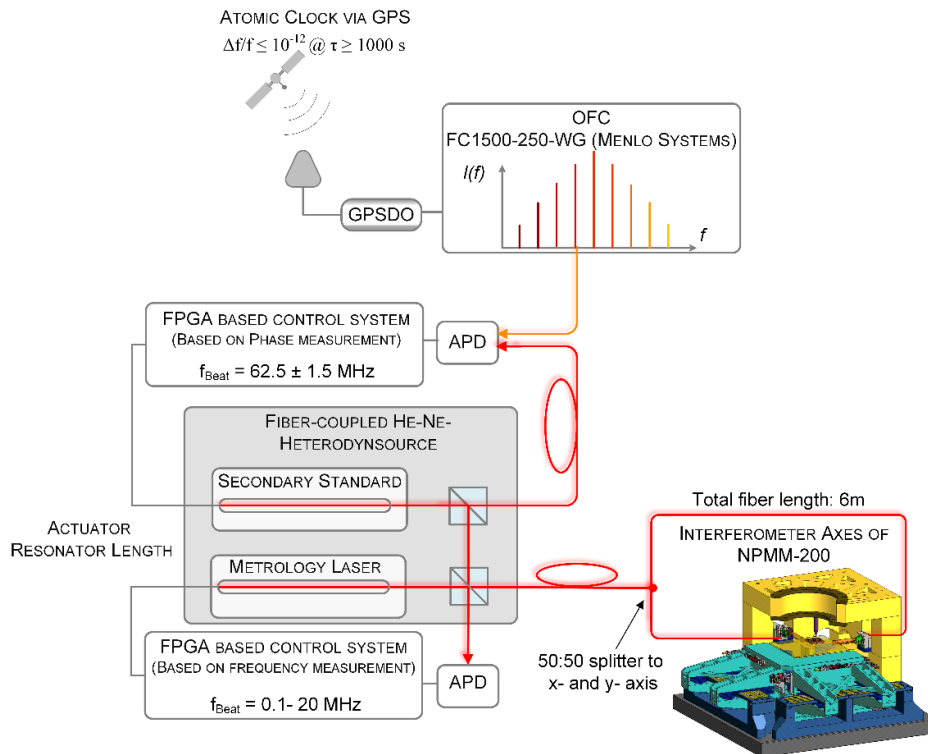


Fig. 1: Schematic of the basic setup for locking the metrology lasers of the NPMM-200 to a single mode of an optical frequency comb. Abbreviations are explained in the text.

3. Results

In fig. 2a) the deviation of the beat signal from its mean value (Δf_{beat}) between the secondary standard (SS) and an optical comb mode prior and after locking the SS to the comb line is shown. The grey curve shows the SS

in its internal stabilization regime based on a two-mode comparison. In this case the frequency comb serves as a stable reference laser and the frequency fluctuations are completely determined by the SS. The maximum frequency deviation within a time window of 24 h can reach up to 1.1 MHz ($2.3 \cdot 10^{-9}$). The resulting relative Allan-deviation is presented in fig. 2c) and shows a distinct increase for integration times higher than 100 s. When locked to the comb line the frequency fluctuations of the SS are eliminated (light blue curve in fig. 2a)). In this case the beat signal indicates how the SS follows the comb line. The same is true for the metrology laser (ML) that is depicted as a dark blue line in fig. 2b). The frequency deviation of these two beat signals mainly depends on the chosen control parameters of the two servo loops used to lock the He-Ne lasers to the comb line. The chosen data in fig. 2b) possesses a maximum frequency deviation of 2.3 kHz (176 Hz) over a time window of 1h for the SS (ML) corresponding to a relative frequency deviation of $4.8 \cdot 10^{-12}$ ($3.7 \cdot 10^{-13}$). The corresponding relative Allan deviations are shown in fig. 2c). The red curve indicates the frequency stability of the OFC limited by the frequency stability of the GPSDO that is used to reference the comb [9]. As can be seen in fig 2c) the relative Allan deviation of the locked SS and ML fall below the Allan deviations of the comb line. This demonstrates that the SS and ML are able to follow the comb line properly. For an integration time of 10 000 s the relative Allan deviation of the comb falls down to $5 \cdot 10^{-13}$. Compared to the internally stabilized He-Ne-lasers with a relative Allan deviation of $4 \cdot 10^{-10}$ at the same integration time an increase in longterm stability of three orders of magnitude can be achieved.

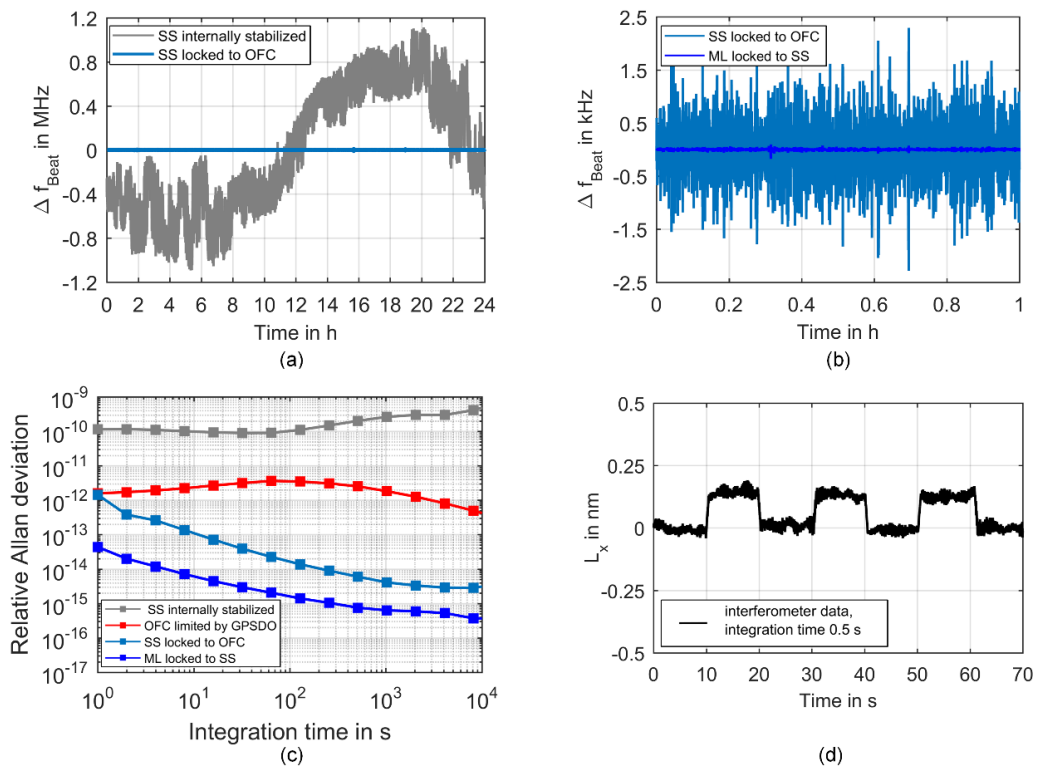


Fig. 2: Frequency stability of a comb-referenced metrology laser. a) Deviation of the beat frequency between the Secondary standard (SS) and a comb line prior and after locking the SS onto the comb line, b) Deviation of the beat frequencies between the SS and a comb line as well as the metrology laser (ML) and the SS when locked to the comb line, c) Respective relative Allan deviations and d) Influence of frequency changes on the interferometric length measurement demonstrated with the comb-referenced metrology laser.

In fig. 2d) the influence of frequency distortions on the length measurements in the NPMM-200 is finally demonstrated by using the comb-referenced metrology lasers. The metrology laser was fed to the x-interferometer axis of the NPMM-200 and the beat frequency between the metrology laser and secondary standard was intentionally changed at a constant position of the positioning stage of 100 mm. Therefor the drive system of the NPMM-200 was deactivated and the positioning stage was mechanically fixed. The introduced frequency jumps of 625 kHz should cause an ostensible length change of 132 pm at a measurement length of 100 mm. As can be seen in fig. 2d) these frequency jumps can clearly be resolved in the length data obtained

from the interferometers where an average length change of $\Delta L_{\text{mean}} = 133.5$ pm with a standard deviation of 9.9 pm was obtained.

4. Conclusion

Ultrastable traceable laser sources for interferometric length measurements in nanopositioning and measuring machines are gaining more importance as the positioning ranges of those machines are steadily increasing. Currently the largest of these machines at the TU Ilmenau is the NPMM-200 which provides a measurement range of 200 mm x 200 mm x 25 mm. Using the approach of a comb-referenced metrology laser it is possible to create a direct and permanent link of the interferometric length measurement within the NPMM-200 to an atomic clock. This way additionally the longterm stability of an individual comb line can be transferred onto the metrology laser. Nevertheless the resulting high frequency stability of better than 10^{-12} can currently only be achieved for integration times longer than 1000 s. Since high positioning dynamics require a high short-term stability (usually integration times below 1s) as well, future work will concentrate on extending this high stability performance into the kHz range.

Acknowledgements

The authors gratefully acknowledge financial support from the Carl-Zeiss-Stiftung as part of the research project “MetroBase”. We thank Menlo Systems for the frequency stability data of the GPSDO presented in fig. 2c.

References

1. G. Jäger, “Nanopositioning and nanomeasuring machine NPMM-200 – a new powerful tool for large-range micro- and nanotechnology,” *Surf. Topogr.: Metrol. Prop.*, 4, 034004, 2016.
2. I. Ortlepp, “Tip- and laser-based 3D-Nanofabrication in extended macroscopic working areas”, accepted for Nanomanufacturing and Metrology, 2021.
3. E. Manske, “Progress of nanopositioning and nanomeasuring machines for cross-scale measurement with sub-nanometre precision”, *Meas. Sci. Technol.* 31, 085005, 2020.
4. T. M. Niebauer, “Frequency stability measurements on polarization-stabilized He-Ne lasers”, *Applied Optics* vol. 27, pp. 1285-1289, 1988.
5. F. Riehle, “The CIPM list of recommended frequency standard values: guidelines and procedures”, *Metrologia*, vol. 55, no. 2, pp. 188-200, 2018.
6. P. Köchert, “Ultrastable metrology laser at 633 nm using an optical frequency comb,” in *Optical Micro- and Nanometrology VII. International Society for Optics and Photonics*, Strasbourg, France, 2018, 106780S.
7. Menlo Systems, “GPS-8 10 MHz RF Reference”, User Manual, Menlo Systems GmbH, Munich, Germany, 2016.
8. C. Sternkopf, “Digitally frequency offset-locked He-Ne laser system with high beat frequency stability, narrow optical linewidth and optical fibre output”, *Meas. Sci. Technol.* 29, 064013, 2018.
9. J. Kim, “Ultralow-noise mode-locked fiber lasers and frequency combs: principles, status, and applications”, *Advances in Optics and Photonics*, vol. 8, pp. 465-540, 2016.

The effect of particle loading, surfactant concentration and sonication time on the wettability of multi-walled carbon nanotubes based nanofluid

Mohamed Abubakr¹, T .A. Osman², Hossam A. Kishawy³, Hussien Hegab³, A.M.K. Esawi^{1*}

¹Department of Mechanical Engineering, The American University in Cairo (AUC), AUC Avenue, P.O. Box 74, New Cairo 11835, Egypt

²Mechanical Design and Production Engineering Department, Cairo University, Giza 12613, Egypt.

³Machining Research Laboratory, Ontario Tech.University, Oshawa, ON L1G 0C5, Canada.

Abstract:

The wettability aspect of the multi-walled carbon nanotubes (MWCNTs) based nanofluid was investigated for different nanoparticle MWCNTs concentration, sonication times, and surfactant concentrations. The wettability was experimentally evaluated using the contact angle method based on L9OA orthogonal array. The analysis of variance (ANOVA) showed that the MWCNT loading is the most influential factor followed by surfactant concentration and sonication time, respectively. Besides, the contact angle was found to be increased with increasing the MWCNTs concentration. However, decreasing the surfactant concentration increases the contact angle. This study provides insights about the underlying physical mechanism of nanofluid wettability and makes progress towards solving the conflicting theories proposed in the open literature.

Keywords: Nanofluids, MWCNTs, Wettability, Contact angle, Mechanisms.

Nomenclature

L9OA	Latin hypercube orthogonal array
MWCNT	Multi-wall carbon nanotubes
NF	Nano fluid
NP	Nanoparticles
SWCNT	Single wall carbon nanotubes

1. Introduction

Nanofluids are now considered as an ultra-high performance fluid in different applications. This is due to their unique thermo-physical properties. One of these properties is nanofluid wettability, which defines nanofluid spreading on a given surface. The addition of nanoscaled particles is known to significantly alter this property (Estellé et al. 2018). This has been reported in different studies in the open literature. However, it is not globally agreed upon whether the nanoparticle addition is enhancing or hindering the fluid spreading. This is evident from the contradicting reported trends in the open literature. One reason for this global inconsistency is the discrepancy in the reported mechanism and theories behind the role of nanoparticles in nanofluid wettability.

Three reoccurring theories for nanoparticles' role in nanofluid wettability are related to (1) the intermolecular force (cohesion) manipulation due to the addition of nanoparticles (Lu, Duan, and Wang 2014; Karthikeyan, Coulombe, and Kietzig 2017; Harikrishnan et al. 2017). (2) surface modification due to the deposition of nanoparticles and its effect on contact line dynamics. (Sefiane, Skilling, and MacGillivray 2008; Radiom, Yang, and Chan 2010) (3) the intermolecular force manipulation due to the existence of surfactant molecules associated with the added nanoparticles (Ranjbar et al. 2015; Kumar and Milanova 2009). In general, the wettability of nanofluid has not been focused on compared to other physical properties in the literature. Moreover, there are very few studies, if any, on MWCNT, in particular. In one of the studies, it was found that the addition of single-wall carbon nanotube (SWCNT) to water increased surface tension while increasing the

* Corresponding author: Tel.: +20 2 26153102. E-mail address: a_esawi@aucegypt.edu (A.M.K. Esawi).

surfactant showed the opposite effect (Kumar and Milanova 2009). On the contrary, the contact angle was found to be negatively correlated to the MWCNT volume concentration for palm oil seeded with MWCNT nanofluids (Li et al. 2017). The results from these two studies are showing contradicting effects, and no underlying theories were provided. On the other side, the Van der-Waal’s force between NP on the gas-liquid interface was held responsible for increasing the surface tension on MWCNT seeded fuels (Tanvir and Qiao 2012).

Based on the reviewed literature, a very limited number of studies have addressed the effect of MWCNT on nanofluid wettability. This number is even less for the effect of surfactant concentration, and to the best authors’ knowledge, no studies have been conducted on the effect of sonication time on wettability. In this study, these three factors are experimentally investigated, and a new mechanism has been proposed to explain them. Besides, the reported experimental finding has also been used to evaluate the applicability of the existing theories in the literature. The work proposed in this study aims to a better understanding of the wettability characteristics of MWCNT nanofluid by assessing the contribution of the diverse proposed mechanism in the open literature.

2. Experimentation

In this study, both mechanical (i.e., sonication and stirring) and noncovalent techniques (surfactant) were applied for stabilization. Since the utilized base fluid is organic (vegetable oil), non-ionic surfactant (Triton X from Sigma Aldrich) was used. Elicarb MWCNT purchased from Thomson Swan (UK) with an average diameter between 10-12 nm, and lengths of tens of microns were used in the present study. The nanofluid was prepared via two steps sonication to prompt the unzipping mechanism (Strano et al. 2003) and assure uniform surfactant adsorption on the MWCNT surface.

The contact angle was measured using KRUSS drop shape analyzer 25B. A constant volume of 10 μ l (microliter) was dispensed using a micro-syringe, and measurements were repeated at least nine times for every sample. All measurements were taken after one minute of placing the droplet on the surface. The same surface and pre-conditioning procedures were used for all samples to eliminate any noise in the results. In this analysis, the effects of three control factors, nanoparticle (NP) loadings, sonication times, and surfactant concentrations, on the contact angle were investigated utilizing the L9OA design, as shown in Table 1. The relation between the control factors and the contact angle was computed by using the response graph (Main effect plot) (Montgomery 2012).

Table 1: Experiment array and corresponding contact angle

Run	MWCNT Loading (X) (ml MWCNT per ml oil %)	Sonication Time (Y) (min)	Surfactant Concentration (Z) (gm surfactant per gm MWCNT)	Contact angle (Degree)
1	0.1	5	0	22
2	0.1	10	0.1	25
3	0.1	30	10	17
4	0.4	5	0.1	30.6
5	0.4	10	10	28
6	0.4	30	0	40
7	0.7	5	10	30
8	0.7	10	0	35
9	0.7	30	0.1	37

3. Results and Discussion

In this section, the contact angle measurements in Table 1 are analyzed. The main effect plot in Figure 1 is used to show the correlation between each of the three studied control factors and the contact angle.

Figure 1 (a) shows that the increase of nanoparticle loading caused an increase in the contact angle. The 0.7% NP loading led to a 37.2% higher contact angle compared to the 0.1% loading. The exact mechanism which controls the influence of nanoparticles on the contact angle is not agreed upon. The contact angle is directly related to surface tension, which is a force generated from the cohesion between fluid molecules working on

minimizing the surface of a given droplet volume. The increase in contact angle indicates an increase in this force. Many theories have tried to relate the addition of nanoparticles and the change in this force. In the next part, the applicability of these theories on the current experimental finding will be discussed.

A cohesion-related theory was proposed for functionalized nanoparticles in polar solutions (Karthikeyan, Coulombe, and Kietzig 2017). The argument in this theory is based on the fact that functionalized groups attached to the surface of MWCNTs lead to increasing the attraction force (cohesion) between the polar solution molecules. This cohesion leads to an increase in the surface tension and can be attributed to the increase in contact angle as the nanoparticle loading increases. Since un-functionalized nanoparticles (as in the current study) showed an increase in contact angle, then the effect of functional groups could not be solely responsible for this increase in contact angle and surface tension, and it does not apply to the current experimental findings.

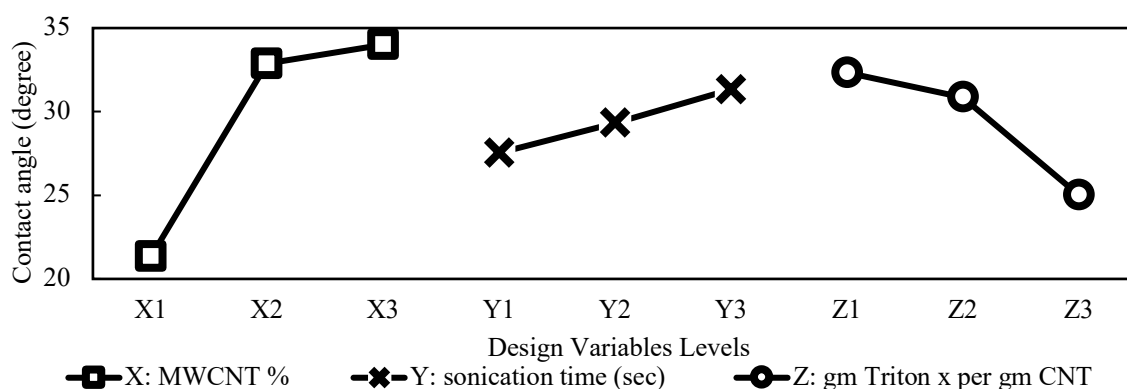


Figure 1: Main effect plot of control factors on the contact angle

However, cohesion from the functionalization is not applicable in the case of a non-polar solution; another form of attraction between the MWCNT and molecules of a non-polar solution may lead to a similar effect. The existence of nanoparticles in the base fluid is associated with an ordered layer of base fluid molecules around the nanoparticle (Yu and Choi 2003; Xue et al. 2004). The reason behind the generation of this layered fluid is due to the high particle-to-liquid molecule interacting forces. This force leads to attracting and organizing the liquid layer in a strong solid-like structure. Thus, at this ordered layer, liquid particles are forced to get closer, forming a packed organized structure that is difficult to disturb or separate its elements. Such a constrained structure can be thought of as an immobilization mechanism for NF droplet spreading (wettability). This is due to the fact that spreading requires the liquid molecules to be flexible to move around freely and to be re-oriented to form a thin film maximizing the wetted surface area. The effect of forming these ordered nanolayers resembles an extra cohesion force between layered molecules. On the other hand, the extra MWCNT to MWCNT Van der Waal's attraction force will enhance the internal attraction between molecules inside the droplet. Thus, it further works on immobilizing the relative motion between differently formed nanolayers around different MWCNT particles boosting the fluid cohesion and lowering its wettability even more.

Another theory, aside from the increase in cohesion, is related to the contact line dynamics (Radiom, Yang, and Chan 2010). The authors pointed out that the droplet spreading is controlled by the displacement of the contact line on the solid surface. The contact line will spread by moving between absorbing sites until it reaches equilibrium at one of these sites (Blake and De Coninck 2002). Based on this theory, it was postulated that the increase in the contact angle is due to pinning the contact line at these adsorbing sites under the influence of nanoparticles (Radiom, Yang, and Chan 2010). According to this theory, the nanoparticles support the bulk fluid of the droplet and roughen the surface of the solid, leading to a higher contact angle. However, this theory suggests that nanoparticles lead to lower spreading; there are still others that have reported the opposite. It was suggested that the existence of nanoparticles enhances the spreading of contact line by rolling and lubrication effect, thus facilitating spreading and advancing of contact angle (Sefiane, Skilling, and MacGillivray 2008). This point of view is suggested for spherical nanoparticles owing to their high rolling capabilities. The difference in the form (spherical and tubular) might be the reason behind the different effects between the two nanoparticles on contact line dynamics. However, this theory represents a good argument; it is only limited to explain the spreading of a droplet on the surface. In other words, this theory is not applicable to explain the change reported

in the surface tension in various studies (Ranjbar et al. 2015; Wang, Mitrašinović, and Wen 2012) using the pendant drop method, where the droplet is not in contact with any surfaces. This indicates that this theory may be valid in the current case; however, it is not the main contributor to the effect of nanofluids on wettability.

Another theory is built on the fact that the nanoparticles dispersed in a dispersant will experience a collision with the dispersant molecules leading to a series of reflections, forcing particles to move in a random motion, known as Brownian motion. In this theory, the authors reported that the Brownian motion might lead to decreasing the cohesion between fluid molecules and reducing the contact angle (Murshed, Tan, and Nguyen 2008). However, this does not agree with the current experimental finding, as shown in Figure 1. The Figure indicates that adding more nanoparticle increase the contact angle. So even though adding more particles to the fluid increases the collision rate of the nanoparticle due to a higher probability of collision (higher Brownian motion), the contact angle still declines. This indicates that this theory is not applicable in the current case. This is because even though the existence of Brownian motion is an agreed-upon fact and has a considerable effect on altering the physical properties such as the thermal conductivity (Kebinski et al. 2001; Yang and Han 2006), it has been suggested that the Brownian motion role is insignificant in the case of MWCNT. This insignificant role is due to the fact that the aspect ratio of MWCNT is very high (its length is much longer than its diameter), and it has been suggested that the Brownian motion effect tends to fade away for particles like MWCNT (Huaqing et al. 2011; Prasher, Phelan, and Bhattacharya 2006; Yang and Han 2006). This is why reduction of surface tension by Brownian motion is not a valid theory for MWCNT, even though it can be for spherical particles with a small aspect ratio (~ 1). In conclusion, in the current study, the proposed mechanism related to the cohesion enhancement due to nanolayering as well as the contact line pinning proposed in (Radiom, Yang, and Chan 2010) were consistent with the current findings for the effect of nanoparticle loading on the contact angle.

On the other hand, the sonication time and surface amount showed a relatively lower contribution according to the contact angle. The sonication time, Figure 1 (b) shows that increasing sonication time leads to increasing the contact angle. This can be explained by the fact that increasing sonication will (1) decrease the amount of sedimented MWCNT (2) detangling the agglomerates. The first effect resembles adding extra nanoparticles to the solution, which, according to Figure 1 (a), is expected to cause the contact angle to increase. The second effect (detangling the agglomerates) will increase the exposed area of the MWCNT particle. This should enhance both liquid nano-layering and particle to particle van der Waal attraction force. Besides, it can be argued that detangling the agglomerates can improve the contact line pinning theory (Radiom, Yang, and Chan 2010) since more particles could penetrate to adsorption sites and attach to them. So based on this discussion, the small increase in contact angle in Figure 1 (b) (13.8% increase from the 5 min to the 30 min) can be adequately explained by the newly proposed mechanism in this study as well as by the contact line pinning theory (Radiom, Yang, and Chan 2010). Regarding the surfactant effect, Figure 1 (c) shows that increasing the surfactant concentration decreases the contact angle. This is because, in the absence of any nanoparticle, adding a surfactant to the base fluid will lower its surface energy (Kumar and Milanova 2009). Additionally, it works on generating repulsive force between nanoparticles (Tanvir and Qiao 2012), negating the particle to particle cohesion due to van der Waal attraction force.

4. Conclusions

In this study, the effects of the MWCNT loading, sonication time, and surfactant amount were studied. It was found that increasing any of the MWCNT loading or sonication time lead to an increase in the contact angle while increasing the surfactant showed the opposite. A new physical mechanism involved the effect of liquid layering, and Van der Waal attraction force between particles has been proven adequate to explain the current experimental finding. Besides the applicability of other theories related to contact line dynamics, Brownian motion and nanoparticle functional groups have been checked, and the contact line dynamics were proven the most effective among them in the case of MWCNT oil-based nanofluid. This study provides scholars with better-detailed explanations and comparisons between different theories explaining the wettability of nanofluid in general and MWCNT in particular.

Acknowledgments

The authors extend their appreciation to the Egyptian Academy of Scientific Research and Technology (ASRT) for funding this work through JESOUR program.

References

1. Blake, T.D, and J. De Coninck. 2002. "The Influence of Solid–Liquid Interactions on Dynamic Wetting." *Advances in Colloid and Interface Science* 96 (1–3): 21–36. [https://doi.org/10.1016/S0001-8686\(01\)00073-2](https://doi.org/10.1016/S0001-8686(01)00073-2).
2. Estellé, Patrice, David Cabaleiro, Gawel Żyła, Luis Lugo, and S. M.Sohel Murshed. 2018. "Current Trends in Surface Tension and Wetting Behavior of Nanofluids." *Renewable and Sustainable Energy Reviews* 94 (November 2017): 931–44. <https://doi.org/10.1016/j.rser.2018.07.006>.
3. Harikrishnan, A. R., Purbarun Dhar, Prabhat K. Agnihotri, Sateesh Gedupudi, and Sarit K. Das. 2017. "Effects of Interplay of Nanoparticles, Surfactants and Base Fluid on the Surface Tension of Nanocolloids." *European Physical Journal E* 40 (5): 16–23. <https://doi.org/10.1140/epje/i2017-11541-5>.
4. Huaqing, X., Y. Wei, L. Yang, and C. Lifei. 2011. "Discussion on the Thermal Conductivity Enhancement of Nanofluids." *Nanoscale Research Letters* 6: 1–12. <https://doi.org/10.1186/1556-276X-6-124>.
5. Karthikeyan, A, Sylvain Coulombe, and A M Kietzig. 2017. "Wetting Behavior of Multi-Walled Carbon Nanotube Nanofluids." *Nanotechnology* 28 (10): 105706. <https://doi.org/10.1088/1361-6528/aa5a5f>.
6. Keblinski, P., S. R. Phillpot, S. U S Choi, and J. A. Eastman. 2001. "Mechanisms of Heat Flow in Suspensions of Nano-Sized Particles (Nanofluids)." *International Journal of Heat and Mass Transfer*. [https://doi.org/10.1016/S0017-9310\(01\)00175-2](https://doi.org/10.1016/S0017-9310(01)00175-2).
7. Kumar, Ranganathan, and Denitsa Milanova. 2009. "Effect of Surface Tension on Nanotube Nanofluids." *Applied Physics Letters* 94 (7): 18–21. <https://doi.org/10.1063/1.3085766>.
8. Li, Benkai, Changhe Li, Yanbin Zhang, Yaogang Wang, Min Yang, Dongzhou Jia, Naiqing Zhang, and Qidong Wu. 2017. "Effect of the Physical Properties of Different Vegetable Oil-Based Nanofluids on MQLC Grinding Temperature of Ni-Based Alloy." *International Journal of Advanced Manufacturing Technology* 89 (9–12): 3459–74. <https://doi.org/10.1007/s00170-016-9324-7>.
9. Lu, Gui, Yuan Yuan Duan, and Xiao Dong Wang. 2014. "Surface Tension, Viscosity, and Rheology of Water-Based Nanofluids: A Microscopic Interpretation on the Molecular Level." *Journal of Nanoparticle Research* 16 (9). <https://doi.org/10.1007/s11051-014-2564-2>.
10. Montgomery, Douglas C. 2012. *Design and Analysis of Experiments Eighth Edition*. Design. <https://doi.org/10.1198/tech.2006.s372>.
11. Murshed, S. M.Sohel, Say Hwa Tan, and Nam Trung Nguyen. 2008. "Temperature Dependence of Interfacial Properties and Viscosity of Nanofluids for Droplet-Based Microfluidics." *Journal of Physics D: Applied Physics* 41 (8). <https://doi.org/10.1088/0022-3727/41/8/085502>.
12. Prasher, Ravi, Patrick E. Phelan, and Prajesh Bhattacharya. 2006. "Effect of Aggregation Kinetics on the Thermal Conductivity of Nanoscale Colloidal Solutions (Nanofluid)." *Nano Letters* 6 (7): 1529–34. <https://doi.org/10.1021/nl060992s>.
13. Radiom, Milad, Chun Yang, and Weng Kong Chan. 2010. "Characterization of Surface Tension and Contact Angle of Nanofluids." *Fourth International Conference on Experimental Mechanics* 7522 (December): 75221D. <https://doi.org/10.1117/12.851278>.
14. Ranjbar, Hemat, Mohammad Reza Khosravi-Nikou, Amir Safiri, Samaneh Bovard, and Ali Khazaei. 2015. "Experimental and Theoretical Investigation on Nano-Fluid Surface Tension." *Journal of Natural Gas Science and Engineering* 27: 1806–13. <https://doi.org/10.1016/j.jngse.2015.11.010>.
15. Sefiane, Khellil, Jennifer Skilling, and Jamie MacGillivray. 2008. "Contact Line Motion and Dynamic Wetting of Nanofluid Solutions." *Advances in Colloid and Interface Science* 138 (2): 101–20. <https://doi.org/10.1016/j.cis.2007.12.003>.
16. Strano, Michael S., Valerie C. Moore, Michael K. Miller, Mathew J. Allen, Erik H. Haroz, Carter Kittrell, Robert H. Hauge, and R. E. Smalley. 2003. "The Role of Surfactant Adsorption during Ultrasonication in the Dispersion of Single-Walled Carbon Nanotubes." *Journal of Nanoscience and Nanotechnology* 3 (1): 81–86. <https://doi.org/10.1166/jnn.2003.194>.
17. Tanvir, Saad, and Li Qiao. 2012. "Surface Tension of Nanofluid-Type Fuels Containing Suspended

- Nanomaterials.” *Nanoscale Research Letters* 7 (1): 226. <https://doi.org/10.1186/1556-276X-7-226>.
18. Wang, Zhen Tao, Aleksandar M. Mitrašinić, and John Z. Wen. 2012. “Investigation on Electrostatic Breakup of Bio-Oil Droplets.” *Energies* 5 (11): 4323–39. <https://doi.org/10.3390/en5114323>.
 19. Xue, L., P. Keblinski, S. R. Phillpot, S. U.S. Choi, and J. A. Eastman. 2004. “Effect of Liquid Layering at the Liquid-Solid Interface on Thermal Transport.” *International Journal of Heat and Mass Transfer* 47 (19–20): 4277–84. <https://doi.org/10.1016/j.ijheatmasstransfer.2004.05.016>.
 20. Yang, B., and Z. H. Han. 2006. “Temperature-Dependent Thermal Conductivity of Nanorod-Based Nanofluids.” *Applied Physics Letters* 89 (8): 1–4. <https://doi.org/10.1063/1.2338424>.
 21. Yu, W., and S.U.S. Choi. 2003. “The Role of Interfacial Layers in the Enhanced Thermal Conductivity of Nanofluids: A Renovated Maxwell Model.” *Journal of Nanoparticle Research* 5 (1/2): 167–71. <https://doi.org/10.1023/A:1024438603801>.

Influence of element composition on thermal stability and oxidation resistance of Ti-Cr-Mo-Ni-N coatings

Alexey Chernogor¹, Igor Blinkov¹, Alexey Volkhonskiy¹

¹Functional nanosystems and high-temperature materials, NUST “MISIS”, Moscow, Russia
Leninsky prospekt 4, Moscow, Russia, avchernogor@misis.ru

Abstract

In this work, the thermal stability and heat resistance of the Ti-Cr-N, Ti-Cr-N-Ni and Ti-Cr-Mo-N-Ni arc-PVD coatings were studied. Coatings with a high titanium content are prone to rapid oxidation. An oxide film is formed on the surface of the coatings, consisting of TiO₂ and Cr₂O₃. At concentrations of 8% Ti and 42% Cr, the coatings retain their structure, and the thickness of the oxide film is less than 100 nm. To study thermal stability, all samples were subjected to high-temperature annealing in vacuum at temperatures of 650 and 850 °C. Due to the high solubility of TiN and CrN nitrides, the structure of TiCrN and TiCrNiN coatings degrades over the entire temperature range. The introduction of nickel with a concentration of 2.5% into the Ti-Cr-Ni-Mo-N, as well as molybdenum, which forms nitrides with a relatively low solubility in titanium and chromium nitrides, increases the thermal stability of the coatings.

Keywords: arc-PVD, nitrides, thermal stability, ceramics, coatings, thin films, wear

1. Introduction

Nowadays multicomponent coatings based on nitrides of transition metals are actively studied. This interest is associated with the high and unique properties of coatings that can be obtained. Of particular interest are the (Me,Me)N-Ni/Cu systems, where, because of the complete solubility of the components in each other, nitride grains of alternating compositions are formed in the nickel matrix. In this work, the thermal stability and heat resistance of the Ti-Cr-N, Ti-Cr-N-Ni and Ti-Cr-Mo-N-Ni systems prepared by the arc-PVD method were studied.

2. Methods

The investigated Ti-Cr-N, Ti-Cr-Ni-N and Ti-Cr-Ni-Mo-N coatings were prepared by the arc-PVD method. The deposition of coatings was carried out on a unit equipped with three evaporators, described in detail in the work [1, 2]. X-ray phase analysis was carried out on a D8Discover device from Bruker AXS. A copper anode with a wavelength of 0.154186 nm was used as electron radiation. The survey was carried out at a fixed angle of 3 degrees using the sliding geometry method and a step of 0.01°. The macro stress of the coatings was studied by the $\sin^2\psi$ method at an angle of 2 degrees. The binding energy and composition of the coatings were studied by X-ray photoelectron spectroscopy (XPS) on a VersaProbeII spectrometer (ULVAC-PHI). Monochromatic AlK α radiation with a power of 25 W was used to excite the photoemission. The diameter of the analysis area was 100 μ m. High-resolution spectra were recorded at a transmission energy of 11.75 eV and a data acquisition density of 0.1 eV/step. The elemental composition, surface morphology before and after oxidation were studied using a scanning electron microscope equipped with X-Ray spectroscopy. Structural transformations and phase analysis were investigated by transmission electron microscopy. Thin lamellas of the EK61 alloy coating prepared by ion etching were used as samples.

3. Results and Discussion

Coatings composition before and after oxidation presented at table 1. It can be seen that the samples of the Ti-Cr-N and Ti-Cr-N-Ni systems undergo the greatest oxidation compare to Ti-Cr-Mo-Ni-N coatings. It is possible that the high heat resistance of the coatings of the third system is associated with a large amount of chromium [3, 4].

Table 1: Element composition of coatings before and after oxidation at 650 °C

Coating	Element concentration, at. %					
	Cr	Ti	N	Ni	Mo	O
Ti _{0,43} Cr _{0,57} N _{0,89}	23,0	19,5	33,9	-	-	19,8
Ti _{0,34} Cr _{0,66} N _{0,75} – 0,1 Ni	28,7	18,3	33,0	1,5	-	19,6
Ti _{0,15} Cr _{0,85} N _{0,75} -Mo ₂ N – 2,5 Ni	41,7	6,5	39,4	1,5	7,3	3,6

The data of X-ray microanalysis are also confirmed by the concentration profiles of the coatings after oxidation and X-Ray diffraction. After oxidation of TiCrN coatings phase composition of the coatings includes Cr₂O₃ and TiO₂, the appearance of titanium oxide indicates destructive oxidation [5]. According to the profiles, presented on figure 2, on the surface the ratio of titanium and oxygen concentrations corresponds to the TiO₂ phase. Since it is characterized by high oxygen permeability, it can be assumed that with prolonged annealing, the depth of the oxide layer will continue to increase up to the substrate. With an increase in the chromium concentration to 36% and 42% in the Ti_{0,34}Cr_{0,66}N_{0,75} – 0,1 Ni and TiCrMoN-2.5% Ni coatings, respectively, the thickness of the oxide layer is already less than 100 nm. At the same time, oxygen practically does not diffuse into the coating, which indicates the high heat resistance of these coatings.

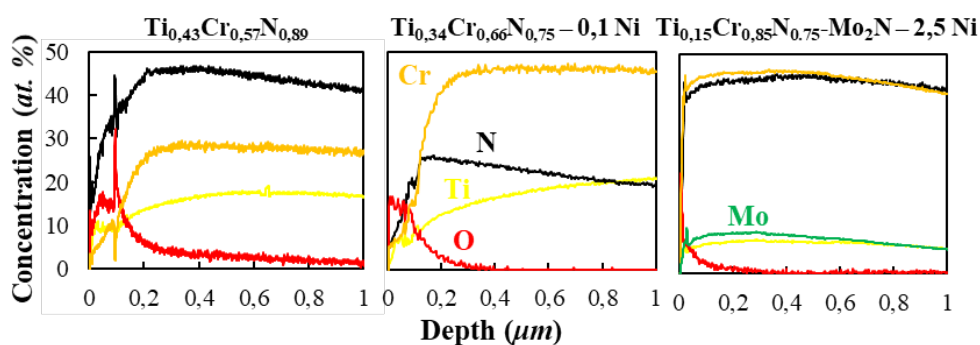
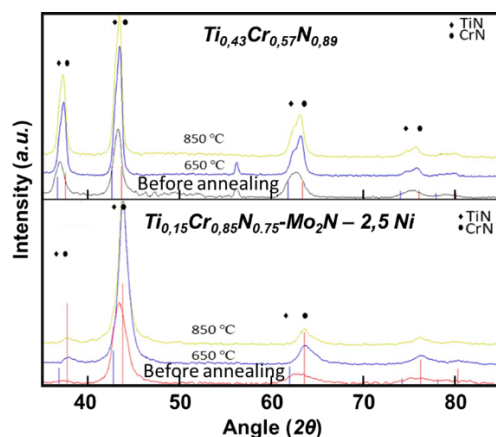
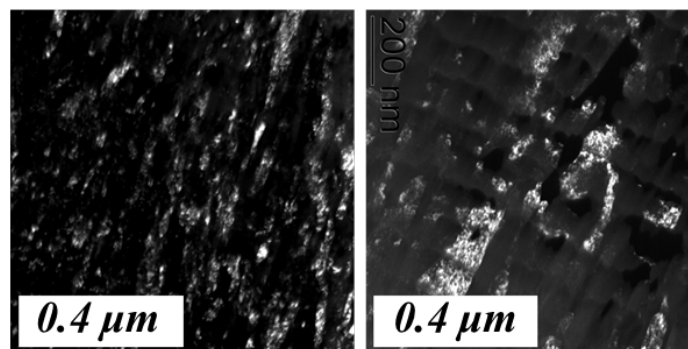


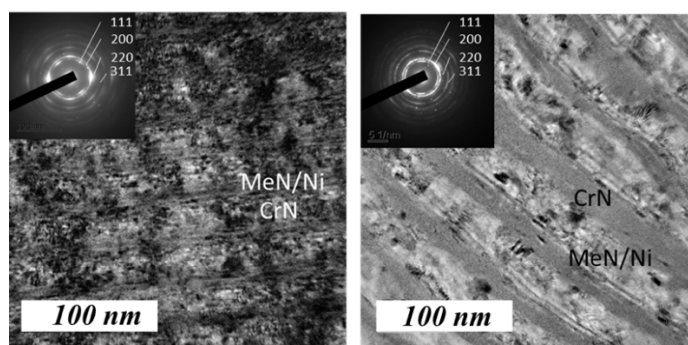
Fig. 1: Concentration profiles after oxidation at 650 °C

To study thermal stability, all samples were subjected to high-temperature annealing in vacuum at temperatures of 650 and 850 °C. For TiCrN and TiCrN-Ni samples with a low nickel content, the splitting of diffraction lines during annealing is observed in the diffraction patterns (fig. 2). This is due to the processes of mutual dissolution of nitrides in each other with the formation of phases enriched in titanium and chromium. In this case, in the process of annealing, recrystallization occurs because of the decomposition of nitride grains into nitrides enriched in titanium and chromium (fig.3). For the Ti_{0,15}Cr_{0,85}N_{0,75}-Mo₂N – 2,5 Ni coating, the diffraction pattern did not reveal the splitting of the diffraction lines; however, there is a clear tendency to the formation of one diffraction line from the CrN phase in the coating.





In addition, the performed TEM analysis (figure 3) for TiCrMoN-Ni coatings established that the layered structure of the coatings is preserved after annealing, while the modulation period for all coatings after annealing approximately corresponds to the modulation period before annealing. This indicates the absence of processes of dissolution of layers in each other. Nevertheless, structural transformations occur within one layer, which consist in the formation of single-crystal sublayers. According to the calculations of the plasma flow, these layers correspond to the layers enriched in chromium, that is, formed by direct passage of the substrates opposite the evaporator with a chromium cathode. Taking into account the XRD and TEM data, it can be assumed that during annealing, chromium diffuses into chromium-enriched sublayers with the formation of the CrN phase, as well as the growth of these nitride grains. Consequently, the broadening of the diffraction lines, which were observed before annealing, is associated with the formation of $\text{Cr}_{1-x}\text{Me}_x\text{N}$ phases in the coating, where x depends on the position of the substrates in the coordinates of the rotating table. The phases enriched in titanium and molybdenum are, in all likelihood, X-ray amorphous. These data clearly demonstrate the role of nickel in the thermal stability of coatings. Since nickel is present only in sublayers formed by passing the substrates opposite the Mo evaporator and, to a greater extent, TiNi. Nickel tends to form an X-ray amorphous shell around nitride grains, which serves as a diffusion barrier during the recrystallization of coatings during the entire annealing [6].



Acknowledgements

The financial support by the Russian Science Foundation Program (Research Project No. 19-19- 00555) is gratefully acknowledged.

References

1. A. Chernogor, I. Blinkov and A. Demirov, "A Study of the Processes of Structure Formation in Ceramic Coatings by the Kinetic Monte Carlo Method", *Technical Physics Letters*, vol. 46, no. 11, pp. 1053-1056, 2020.
2. A. Chernogor, I. Blinkov, D. Belov, V. Sergevnin and A. Volkhonskii, "Analysis of the Structure of Multilayer Nanocrystalline Coatings Based on Plasma Mass Transfer Parameters Calculated by the Monte Carlo Method", *Technical Physics Letters*, vol. 45, no. 2, pp. 75-78, 2019.
3. P. Panjan, B. Navinšek, A. Cvelbar, A. Zalar and I. Milošev, "Oxidation of TiN, ZrN, TiZrN, CrN, TiCrN and TiN/CrN multilayer hard coatings reactively sputtered at low temperature", *Thin Solid Films*, vol. 281-282, pp. 298-301, 1996.
4. D. Lee, M. Kim, Y. Lee and S. Kwon, "High temperature oxidation of TiCrN coatings deposited on a steel substrate by ion plating", *Surface and Coatings Technology*, vol. 141, no. 2-3, pp. 232-239, 2001.
5. F. Aliaj, N. Sylá, T. Dilo and H. Oettel, "Oxidation behaviour of TiN coatings deposited onto unheated grade 1060 steel substrates by reactive d.c. magnetron sputtering", *Proceedings of The 4th Global Virtual Conference*, 2016.
6. D. Belov et al., "Thermal stability and chemical resistance of (Ti,Al)N-Cu and (Ti,Al)N-Ni metal-ceramic nanostructured coatings", *Applied Surface Science*, vol. 388, pp. 2-12, 2016.

Integrated approach for exposure and health effects monitoring of engineered nanomaterials in workplaces and urban areas

A. Progiou¹, E. Bergamaschi², I. Guseva Canu³, C. Creze³, C. Fito⁴, P. Dohanyosova⁵, A.M. Zarogianni⁶, J. Friesl⁷

¹ AXON Enviro-Group, 18 Troias str., Athens, Greece, ap@axonenviro.gr

² Laboratory of Toxicology and Industrial Epidemiology, Department of Public Health and Pediatrics, University of Torino, Torino, Italy, enrico.bergamaschi@unito.it

³ Unisanté, University of Lausanne, Switzerland, irina.guseva-canu@unisante.ch

⁴ Instituto Tecnológico del Embalaje, Transporte y Logística (ITENE), Valencia, Spain, carlos.fito@itene.com

⁵ RAMEM, Madrid, Spain, p.dohanyosova@ramem.com

⁶ Natural Environment and Climate Change Agency, Athens, Greece, a.zarogiani@prv.ypeka.gr

⁷ Yordas GmbH, Forchheim, Germany, j.friesl@yordasgroup.com

Abstract

The aim of the present work, in the framework of the LIFE project NanoExplore, is to develop and demonstrate the feasibility of an integrated approach to conduct biomonitoring studies, characterize exposure levels and elucidate possible health effects deriving from exposure to engineered nanomaterials (ENM) in indoor workplaces and urban areas. This approach addresses current environmental, health, and safety questions about ENMs, by considering the integration of human biomonitoring studies with measured data on particle number concentrations (PNC), mass and particle size distributions (PSD) in the personal breathing zone (PBZ) as an instrument for developing consistent risk management guidelines for use by stakeholders from government, industry, NGOs, or the general public. To this aim, relying on a systematic review of the available literature, a panel of candidate biomarkers of nanomaterial exposure and effects via inhalation has been identified and biomonitoring studies for assessing possible health effects were planned. A standardized protocol for harmonizing the approach among the Partner's Countries has been implemented and has gathered the consent of Ethical Committees. In parallel, the design of a wireless sensor network of 20 unattended, low-cost, portable and battery-powered devices that cooperatively monitor the concentration of ENMs and relevant physical environmental conditions in indoor workplaces and urban areas has been implemented. A risk analysis of possible effects on human health deriving from exposure to ENMs will be carried out in 5 case studies and a refinement of currently available Recommended Exposure Limits (REL) for metal oxides and low soluble carbon-based materials will be suggested. In the long-term, the main goal of this study is to reduce potential adverse effects derived from the exposure to ENMs by setting up a harmonized health surveillance system, and support a EU policy for the safe and responsible use of ENMs.

Keywords: ENMs, nanomaterials, biomonitoring studies, biomarkers, risk analysis, health effects, wireless sensor network, exposure levels

1. Introduction

NanoExplore [1] focuses on the possible effects derived from exposure to ENMs, understood as a new type of chemicals of concern, whose properties differ significantly from those of bulk chemicals of the same composition due to their much larger specific surface area and surface activity [2] or much larger deposition rate in the respiratory systems [3], which may lead to unanticipated effects in human health, like pro-inflammatory effects or development of fibrosis and /or cancer [4], as well as to significantly alter ecosystems, causing adverse effects on the metabolism of a living being [5].

The environmental problem targeted is due to the increasing worldwide use of ENMs in products, the lack of information on current exposure levels on both workers and population, and the scarcity of ENMs potential negative effects data on human health and the environment.

The project aims to improve the understanding of levels, nature and possible adverse effects after ENMs

exposure in indoor workplaces and urban areas, considering the integration of human biomonitoring studies with measured data on the Particle Number Concentration (PNC), mass and Particle Size Distributions (PSD) in the Personal Breathing Zone (PBZ) as an instrument for developing consisting risk management guidelines. So, it proposes the implementation of a network of measurement devices for ENMs levels in air together with the use of biomarkers selected and validated to detect early effects on pulmonary and cardio-vascular system.

There is also still a lack of precise recommended exposure measurement strategies which can be easily implemented and generalized. Moreover, data on 8-h time-weighted averages of specific ENMs from (PBZ) samplings is currently lacking, hampering the development of job-exposure matrices for making tentative assessments of the exposure-outcome relationship. Under this context, the exposure assessment approach validated under the project is based on the generation of job-exposure matrices containing large series of data on the concentration of ENMs in the personal breathing zone, area samples (far field measurements), respirable fractions, inhalable fractions and total suspended particles.

Nowadays, WHO and EU are monitoring PM_{2.5} and PM₁₀ and reporting on their negative health effects and their ability to penetrate our lungs and cause respiratory and cardiovascular morbidity and disease. However, there is a lack of data on the effects of PM₁ to deadly diseases like heart attacks, lung cancer, dementia, emphysema, edema and other serious disease, leading to premature death. In this context, projects like LIFE IMPROVE or LIFE NanoMONITOR have started to provide data on the concentration of particles in the nanometer range in relevant outdoor areas. Similarly, current projects conducted under the FP7 and H2020 research programs such as NanoREG, GuideNANO or NanoFASE compiled relevant data on the concentration of ENMs in workplaces. In spite of this, the consideration of the background levels, or background aerosols (BA), is still a limitation.

Therefore, NanoExplore will provide evidence of the potential detrimental effects of UFPs and ENMs on human health, as well as robust devices to measure the exposure, considering a high progress beyond current laboratory measurement devices. Table 2 shows the ENMs specifications considering in the development of that measurement devices.

To date, toxicity of ENMs to aquatic organisms at different trophic levels such as bacteria, algae, and fish has been widely investigated. Growth inhibition parameters and different levels of effect concentrations, uptake, transport and ENMs distribution in various organisms have been reported [6,7]. There is also scientific agreement that ENMs production, use and disposal lead to environmental release of ENM [8], accumulating in soil, water or biota, endangering the health of living organisms and ecosystems [9].

Regarding effects on human health, several adverse effects have been observed for a number of different organs and organ-specific cell lines, including human epidermal cells, human embryo kidney cells and human bronchial cells, causing cellular toxicity [10] and DNA damage [11]. Pulmonary disease and death were observed in mice, as well as dose-dependent inflammatory reactions [12, 13].

Routes of exposure are well characterized, being inhalation the most common one. Dermal is has also been investigated, but studies have shown little to no transdermal ENMs absorption [14]. Recent studies show the most extensive ENMs exposure occurs in the workplace, particularly research laboratories, start-up companies, pilot production facilities, when ENMS are handling.

Therefore, there is an urgent need to provide stakeholders, including regulatory bodies and companies, with an integrated approach to generate robust data on the exposure levels and related health effects, supporting the risk assessment. An adequate evaluation of ENMs is a major concern being addressed by regulatory agencies from all EU Countries, and international organizations (e.g. OECD), in order to ensure that society can benefit from novel applications of nanotechnology, whilst a high level of protection of health, safety and the environment is maintained.

2. Aim and objectives

The project addresses relevant issues related to the European environmental policy and legislation, including 1) the elucidation of possible ENMs adverse effects posed by means of validated biomarkers, 2) the definition of a quantitative exposure limit value for a set of ENMs for workers and the consumers protection, and 3) the

generation of data on the levels of exposure to ENMs in workplaces and urban areas by setting up a robust wireless sensor network for the real-time remote monitoring of the concentration of ENMs. The concept of NanoExplore is shown in Figure 1.

Moreover, the scheduled activities within the project support the implementation of the 7th Environment Action Programme (Union Environment Action Programme to 2020). NanoExplore could be placed in the third key action area of the programme, which covers challenges to human health and wellbeing, such as water pollution, and sets out a long-term vision of a non-toxic environment, proposing to address risks associated with the use of chemicals in products and chemical mixtures. On the other hand, the theme addressed by the project is aligned with the priorities published by the EU NanoSafety Cluster on March, 2017, as well as with the information published in the EUON, launched by EU authorities, where it is stated that ENMs are covered by the same rigorous regulatory framework that ensures the safe use of all chemicals. Within REACH, the EU defines an exposure level below which no adverse effects are expected (DNEL). Under the EU ‘Framework Directive’ (89/391/EC) on occupational health and safety requirements, indicative Occupational Exposure Levels (OELs) have to be applied. Moreover, when substances have hazardous properties, CLP requires them to be notified to ECHA and labelled and packaged so the substances can be used safely.

The overall aim of NanoExplore project is to develop and demonstrate the feasibility of a harmonized approach “model” to monitor nanoparticles and their possible effects deriving from exposure to engineered nanomaterials (ENM) in indoor workplaces and urban areas.

The NanoExplore project builds a harmonized approach to overcome current data gaps and barriers limiting the implementation of REACH regulation and the use of chemical monitoring data in the protection of human health and the environment when dealing with particles in the nanometer range (1-100 nm) by combining **long series of robust data** on the concentration of ENMs measured by a wireless sensor network (WSN) of monitoring devices, **appropriate biomarkers**, and a **tailored designed software** application. This approach addresses current environmental, health, and safety questions about ENMs, providing stakeholders from government, industry, NGOs, or the general public, with reliable data on the concentration and effects of particles in the nanometer range (1-100 nm).

In detail, the specific objectives of the project are:

- To define a panel of **biomarkers** of nanomaterial exposure and effects via inhalation and dermal uptake
- To develop a **wireless sensor network** of unattended, low-cost, portable and battery-powered devices that cooperatively monitor the concentration of ENMs and relevant physical environmental conditions in indoor workplaces and urban areas.
- To develop a **web-based software application** aimed at supporting health surveillance and the acquisition, management and processing of data on the concentration of ENMs monitored by the wireless sensor network in industrial settings and /or relevant urban areas.
- To carry out a **risk analysis of possible effects on human health** deriving from exposure to ENMs in 5 case studies.
- To refine currently available **recommended exposure levels (RELS)** for metal oxides and low soluble carbon based materials.
- To **validate and demonstrate the feasibility of the NanoExplore approach** for the risk assessment of ENMs in Europe by implementing a pilot study in 5 European countries.

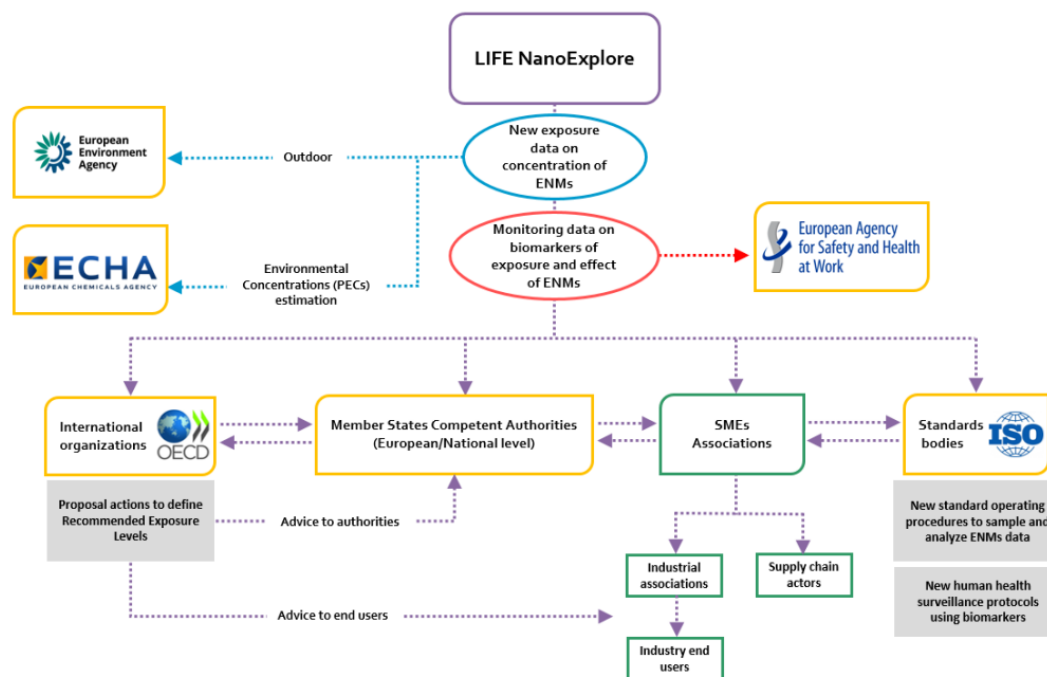


Figure 1: Figure depicting the impact of the project results and the interrelationships between the target audience, stakeholders and the project.

3. Materials and methods

The project includes the following main actions:

3.1 Development of the measuring device

Development of a prototype to collect and measure nanosized and ultra-fine airborne particles from an aerosol stream on a collection plate or filter. To this end, a pump-based sampling system was integrated in the monitoring station. The main characteristics of the monitoring station design and functionality are depicted below:

- a. Compact and portable with a weatherproof box.
- b. Flexible design, subsystems included:
- c. Unattended and remote operation
- d. Battery powered for indoor use and solar cell for outdoor use
- e. Data storage
- f. Ability to provide an appropriate flowrate of the sample to be analysed with TEM grids
- g. Tailored designed software to control the instrument settings
- h. Operation under extreme temperatures -10°C to 40°C
- i. Low-cost.

Considering the system requirements, the selected design concept is based on a “matriuska” concept where some functionalities are in one enclosure and other are in another enclosure. When we need all the functionalities, we can place one enclosure inside the other. The two enclosures are housing the different functionalities listed below

- Indoors enclosure: It has the measurement units and also the electronics to have a totally operative instrument for indoors use, compact, small, with the Human machine interface, the measurement sensors (NP, PM and Particle collection), the functionalities to enter information and the possibility to send data in a wireless manner.
- Outdoors enclosure: This enclosure packs the functionalities needed for outdoor measurements:

- IP65 enclosure with isolation, that is bulky to prevent excessive heating of the sample. It also keeps the screen protected from vandalism.
- Cooling and heating unit: A peltier system, able to keep the temperature of the sensors and electronics in an acceptable range.
- Batteries: Not needed for indoors use since power supply is normally available.
- Solar cell: to feed the batteries in case no power supply is available.

3.2 Development of a web platform

To design and develop the NanoEXPLORE intelligent web-based platform aims at supporting the acquisition, management and processing of data on the concentration of ENMs monitored by the sensor prototype network in industrial settings and the environment. The web-based platform is developed as a private and public hybrid enabler allowing the stakeholders to have their own private space and at the same time some of the data to be accessed by the public.

To ensure reusability of the hybrid web-based platform, a multitenant platform enabling other environmental projects to create their own private virtual space and share their public data with the public was developed.

The Application Development Interface (API) will enable the platform to collect, manage and share data measurements as well as to analyze and display all environmental data in an easy-to-read dashboard and be able to make recommendation based on the information it gets and predictions.

3.3 Validation of candidate biomarkers

Considering candidate biomarkers, a pre-selection of biomarkers applied in air pollution studies related with combustion-derived UFPs [14], as well as of interest on the basis for relevant health endpoints that have been tentatively ascribed to ENMs including cardiovascular, pulmonary, and inflammatory effects: inflammatory biomarkers (e.g. Interleukin 6 - IL-6, Glutathione Peroxidase activity - GPX) and peroxydated products in blood (e.g. eicosanoids, such as 8-isoprostane and LTB4); Oxidative Stress Biomarkers, including oxidation of nucleic acids (8-OHdG, 8-OHG) and of nitrosative stress (3-Cl-Tyr, NO-Tyr) in blood and urine; Pro-inflammatory biomarkers in urine (e.g. Leukotriene); and pulmonary effects biomarkers, including the analysis of CC16 (Clara cell protein) or FENO (Fractional exhaled nitric oxide) in exhaled breath condensate (EBC), and the determination of the Oxidative Potential in Exhaled Air (OPEA), a non-invasive metric related to lung inflammation.



Figure 2: Physical layout of NanoExplore device

3.4 Implementation of field campaigns

The main goal is to conduct a pilot biomonitoring study to assess the feasibility of the harmonised protocol of the collaborative study and refine the NanoExplore integrated approach in a well-characterized limited number of unexposed and exposed workers, including 30 workers from production facilities, 20 workers from office positions, 30 individuals working in civil infrastructures, and 20 control participants.

This task comprises the following subtasks:

- a) Recruitment of the study participants
The standardized protocol including standardized questionnaires translated into corresponding language were applied for worker selection, and inclusion into the study, after obtaining permission from the corresponding national Ethical committees. The expected size of the study population is about 100 workers. For each worker, the following eligibility criteria will be verified:
 - Written consent for participation in the study, inclusion into cohort and follow-up including sampling of EBC, exhaled air and urine.
 - Known occupational exposure to any of the ENMs selected.
 - Suspected exposure to carbonaceous agglomerates (soot and/ or ash) coming mainly from the combustion of engine fuel and lube oil.
 - Availability of medical reports.
 - Availability of information on associated occupational exposures.
 - Availability of information on potential confounding factors.
 - Availability of information on exposure duration and frequency.
 - Isolation from production areas in office positions.
- b) Exposure assessment
This task deals with the characterization of the exposure in the workstations where exposed workers perform the task of concern. ITENE will conduct exposure measuring campaigns to elucidate the nature and extent of the exposure in the Personal Breathing Zone (PBZ).
The main parameters to be reported will be:
 - Number of Particles / cm³
 - Mass concentration in mg/cm³
 - Surface Area in µg/ cm³
 - Particle diameter in nm
 - Particle Size Distribution in nm
 - Mass of NMs / Filter mass in ng/mg of filter
 - Relevant physicochemical information: surface chemistry, agglomeration /aggregation state
- c) Measurement of biomarkers and of their relevance with respect to nanoparticles
This task is focused on the sampling and analysis of the effect biomarkers in biological fluids, including exhaled air, exhaled breath condensate (EBC), urine, buccal epithelium, in order to detect potential early effects on the pulmonary and cardiovascular system.
The samples will be analysed in laboratory. In parallel, the characterization of the health status of workers, creation and completing of a log-book of exposure activities will be performed.
The same biomarkers will be measured twice, considering 6 months between campaign in order to identify any significant difference in any of the biomarkers.
- d) Data validation and statistical analysis of the relationship between nanoparticles exposure and selected biomarkers

3. Results

The main outcome of the project will be an integrated system for the assessment, monitoring and surveillance of the exposure and effects deriving from exposure to engineered nanomaterials (ENM) in indoor workplaces and urban areas, by setting up a new health impact assessment model based on the combination of a wireless sensor, proven biomarkers and a tailored designed software for data acquisition and management. In detail, the expected near-term results are the following:

- A list of 6 prioritized biomarkers of exposure to and effects from nanomaterials in the pulmonary and cardiovascular system to be used in occupational health practice.
- A functional wireless sensor network of 7 unattended, low-cost, portable and battery-powered devices for the real-time remote monitoring of the concentration of ENMs in indoor workplaces and the environment.
- An on-line software application based on a flexible, modular, and extensible client/server architecture to support the access and processing of data on the concentration of ENMs and the continuous collection, analysis and interpretation of health-related data needed for the planning, implementation, and evaluation of public health practice.
- A well-defined list of recommended exposure levels (REL) for metal and metal oxide based ENMs and low solubility carbon based materials.
- A robust European airborne nano-pollutants map useful for epidemiological purposes
- Implementation and demonstration of the applicability and transferability of the health impact assessment model in 5 pilot cases studies, including 2 SMEs, 2 urban areas and one public research organization.
- A complete guidance on the use of human biomonitoring and exposure data in indoor workplaces and the environment for REACH regulation implementation and epidemiological purposes.
- Recommendations for measures and policies to protect worker and population from the health effects of airborne nanopollutants.
- Dissemination actions by means of international conferences, seminars, webinars and workshops to support the training of SMEs, consumers and stakeholders for the sustainable use of ENMs.

In the medium to long-term, the knowledge of the total exposition to ENMs will contribute to healthier lifestyles, and to science-based health and environmental policy at EU Member State and European level. It has been estimated a reduction by a 20 % of diseases related to exposure to ENMs.

Human biomonitoring and wireless sensor networks might become a particularly important tool for decision-makers looking at maximum concentration levels for certain substances, as the case of ENMs.

4. Conclusions

In this work, the environmental problem targeted is due to the increasing worldwide use of ENMs in products, the lack of information on current exposure levels on both workers and population, and the scarcity of ENMs potential negative effects data on human health and the environment.

Recent studies show the most extensive ENMs exposure occurs in the workplace, particularly research laboratories, start-up companies, pilot production facilities, when ENMs are handling. Therefore, there is an urgent need to provide stakeholders, including regulatory bodies and companies, with an integrated approach to generate robust data on the exposure levels and related health effects, supporting the risk assessment.

The NanoExplore project builds a harmonized approach to overcome current data gaps and barriers limiting the implementation of REACH regulation and the use of chemical monitoring data in the protection of human health and the environment when dealing with particles in the nanometer range (1-100 nm) by combining long series of robust data on the concentration of ENMs, measured by a wireless sensor network (WSN) of monitoring devices, appropriate biomarkers, and a tailored designed software application. This approach addresses current environmental, health, and safety questions about ENMs, providing stakeholders from government, industry, NGOs, or the general public, with reliable data on the concentration and effects of particles in the nanometer range (1-100 nm).

Acknowledgements

This work is part funded by the European Commission in the framework of the ENV/GR/000285 LIFE17 Grant Agreement.

References

1. LIFENANOEXPLORE, “Integrated approach for exposure and health effects monitoring of engineered nanomaterials in workplaces and urban areas (LIFE17 ENV/GR/000285),” www.lifenarioexplore.eu, 2021 (accessed: May 23, 2021).
2. S. Hsieh, S. Schubert, C. Hoon, E. Mioshi and J.R Hodges, “Validation of the Addenbrooke's Cognitive Examination III in frontotemporal dementia and Alzheimer's disease,” *Dement Geriatr. Cogn. Disord*, vol.36, pp. 242-250, 2013, <https://doi.org/10.1159/000351671>.
3. R.M. Silva, C. Teesy, L. Franzi, A. Weir, P. Westerhoff, J.E. Evans, K.E. Pinkerton, “Biological response to nano-scale titanium dioxide (TiO₂): role of particle dose, shape, and retention,” *J. Toxicol. Environ. Health A*, vol. 76, pp. 953-972, 2013, 10.1080/15287394.2013.826567.
4. H. Shi, L. Dong, J. Jiang, J. Zhao, G. Zhao, X. Dang, X. Lu and M. Jia, “Chlorogenic acid reduces liver inflammation and fibrosis through inhibition of toll-like receptor 4 signaling pathway,” *Toxicology*, Elsevier, vol. 303, pp 107-114, 2013, <https://doi.org/10.1016/j.tox.2012.10.025>.
5. S. Sauvé and M. Desrosiers, “A review of what is an emerging contaminant,” *Chem. Cent. J.*, vol. 8, pp 15-23, 2014, <https://doi.org/10.1186/1752-153X-8-15>.
6. Z.Wang, X. Xie, J. Zhao, X. Liu, W. Feng, J.C. White, B. Xing, “Xylem- and Phloem-Based Transport of CuO Nanoparticles in Maize (*Zea mays* L.),” *Environ. Sci. Tech.*, vol. 46, pp. 4434-4441, 2012 10.1021/es204212z.
7. R. Kaveh, Y.-S. Li, S. Ranjbar, R. Tehrani, C.L. Brueck, B. Van Aken, “Changes in Arabidopsis thaliana Gene Expression in Response to Silver Nanoparticles and Silver Ions,” *Environ. Sci. Tech.*, vol. 47, pp. 10637-10644, 2013, 10.1021/es402209w.
8. F. Gottschalk, B. Nowack, “The release of engineered nanomaterials to the environment,” *J Environ Monit.*, vol. 13, pp. 1145-115, 2011, 10.1039/c0em00547a.
9. A.R. Köhler, C. Som, A. Helland, F. Gottschalk, “Studying the potential release of carbon nanotubes throughout the application life cycle,” *Journal of Cleaner Production*, vol. 16, pp. 927-937, 2008 <https://doi.org/10.1016/j.jclepro.2007.04.007>.
10. C.M Sayes, A.M. Gobin, K.D. Ausman, J. Mendez, J.L. West, V.L. Colvin, “Nano-C60 cytotoxicity is due to lipid peroxidation,” *Biomaterials*, vol. 26, pp. 7587-7595, 2005, 10.1016/j.biomaterials.2005.05.027.
11. H. K. Lindberg, J. Catalán, K.Aimonen, H. Wolff, I. Wedin, M. Nuopponen, K. Savolainen, H. Norppa, “Evaluation of the genotoxic potential of different types of nanofibrillated celluloses,” in *TechConnect Briefs*, pp. 229–232, 2017.
12. FP7 NanoMICEX-Final Report, Grant agreement ID: 280713, 2015.
13. M Hemmendinger, P. Wild, Y. Shoman, Y., M. Graille, E. Bergamaschi, N. Hopf, I. Guseva Canu, “Reference ranges of oxidative stress biomarkers selected for non-invasive biological surveillance of nanotechnology workers: Study protocol and meta-analysis results for 8-OHdG in exhaled breath condensate.” *Tox Letters*, vol. 327, pp. 41-47, 2020, <https://doi.org/10.1016/j.toxlet.2020.03.021>.
14. MG Bianchi, O. Bussolati, M. Chiu, G. Taurino, E. Bergamaschi, “Evaluation of potential engineered nanomaterials impacts on human health: from risk for workers to impact on consumers,” in: *Exposure to Engineered Nanomaterials in the Environment. Micro and Nano Technologies*, N. Marmiroli, J.C. White, J. Song, Eds. Elsevier Inc., pp. 263-287, 2019, <https://doi.org/10.1016/B978-0-12-814835-8.00010-8>.